Stress amplification in three-dimensional narrow zones created by cavities

Stavros Syngellakis[*]

Abstract

The paper is concerned with a particular case of stress amplification arising from the proximity of a spherical cavity to the boundary of a loaded elastic solid. The performed approximate analysis yields distributions of stresses and displacements in the narrow region formed between a spherical cavity and the faces of a thin flat layer subjected to a far field uniform radial tension. The narrow region is modelled as a circular plate of non-uniform thickness undergoing coupled membrane and flexural deformation. Series solutions are obtained for both membrane forces and bending moments leading to estimates for the stress concentration factor at minimum thickness. These predictions are found consistent with those obtained from both the exact analytical solution and finite element modelling of the problem. Cross-validated results from the two latter methods also provide trends for the stress amplification due to the narrowness of the region.

Keywords: voids, narrow regions, stress concentrations

1 Introduction

Stress concentrations and amplifications around holes and cavities are important indicators of possible material failure in engineering components and structures. They are also linked to void growth and coalescence in porous continua. In the latter case, three-dimensional models of solids with

---

[*]School of Engineering Sciences, University of Southampton, Highfield, Southampton SO17 1BJ, UK, e-mail: ss@soton.ac.uk

spherical or ellipsoidal cavities are certainly more representative of the physical problem rather than the two-dimensional ones for plates or discs with holes. This paper presents approximate solutions for stress concentration and amplification of one such three-dimensional elasticity problem.

Analytical studies of stress concentrations arising from holes or cylindrical cavities in two-dimensional regions can be found in classical Elasticity literature [1]. More recently, attention has turned to the effects of holes in close proximity to each other or to the boundary of a body thus giving rise to narrow regions labelled as ligaments. Approximate solutions [2, 3] exist for such cases yielding the stress concentration factor according to its conventional definition, namely as the ratio of the maximum stress developing at the boundary of the hole to the nominal, mean stress σ_0 over the weakened cross sectional area of the ligament. The mean stress itself is significantly amplified as the width of the ligament tends to zero and recent studies have focused on the order of such amplification for various two-dimensional configurations involving circular holes or cylindrical cavities near the boundaries of stressed regions [4].

In statically determinate problems, the ligament mean stress σ_0 is easily obtained in terms of the far field tension T and the minimum ligament thickness h_0. An interesting, statically indeterminate case arises from the presence of a hole near the straight boundary of the infinite half space. The exact solution of this problem [5, 6] has been studied to provide additional insight into the relation between ligament nominal stress and thickness as the hole approaches the half space boundary [7].

Analytical solutions for solids with spherical cavities, especially when the latter form narrow regions by being very close to the boundary or to each other, are less common due to the complexity of the respective three-dimensional problem. An approximate solution for the stress concentration factor has been obtained in the case of a spherical cavity in a cylindrical bar subjected to remote uniform axial tension as shown in Fig.1 [2]. The narrow region in this problem is a cylindrical shell of variable thickness. The mean stress over the section of minimum thickness can be easily obtained by applying force equilibrium in the axial direction; this gives

$$\sigma_0 = \frac{(R + h_0)^2}{(R + h_0)^2 - R^2} T = ST, \tag{1}$$

where S is the stress amplification factor associated with the narrowness of the region between the cavity and the bar's cylindrical surface.
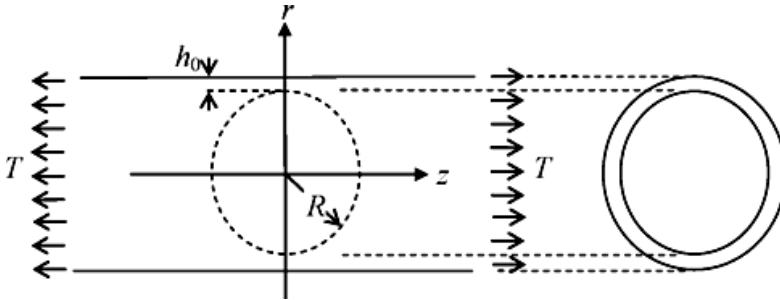
Figure 1: Centrally located spherical cavity in a cylindrical bar under uniform axial tension

For $\delta g = h_0/R << 1$,

$$S \cong \frac{R}{2h_0} = \frac{1}{2\delta}; \tag{2}$$

therefore, S in the thin shell is of the same order of magnitude as in the ligament between a central hole and the edges of a flat strip [4]. The nominal stress is further amplified according to

$$\sigma_{max} = K\sigma_0, \tag{3}$$

where K is the conventional stress concentration factor. Approximate analysis [2] located σ_{max} at the surface of the cavity and produced the expression

$$K = \frac{(6 - 4\nu)(1 + \nu)}{5 - 4\nu^2}, \tag{4}$$

where ν is the Poisson's ratio of the material.

In principle, stress amplification arising from reducing the thickness of the region between voids can be identified by studying the corresponding trends in an existing solution adopting a strategy similar to that employed for the two-dimensional Mindlin problem [8]. A three-dimensional elasticity problem with a known solution to which such a strategy would be applicable is that of two cavities in an infinite elastic medium under remote uniform tri-axial tension [9]; the respective stress and displacements fields are given as infinite series with coefficients obtained from systems of infinite equations. However, it was numerically shown through the solution of truncated systems [9] that the convergence of the stress results is becoming extremely

slow and is eventually lost as the two cavities approach each other; hence it is practically impossible to identify explicit stress magnification trends from that particular analysis. Various such formal, infinite series solutions of other three-dimensional stress concentration problems are cited and discussed in the main body of the paper.

A general strategy, potentially applicable to both two- and three-dimensional problems, was proposed [10] whereby two separate solutions are developed, one for the narrow region, which can be considered as a thin plate or shell, and another for the rest of the solid. The two solutions should be kinematically compatible at the interface between the two regions. This concept has been applied to the problem of assessing stress amplification in the neighbourhood of a large eccentric hole in a strip under tension [3].

In this paper, a particular three-dimensional problem is considered and approximate solutions are obtained for displacements and stresses in its narrow region in the form of infinite series. The narrow region is modelled as a circular plate of variable thickness. The analysis leads to an approximate expression for the stress concentration factor due to the presence of a spherical cavity near the solid boundary. A mathematically rigorous infinite series solution of the overall problem as well as its finite element modelling provide further insight into the validity of theoretical assumptions and results; they also allow the assessment of stress amplification trends as the thickness of the narrow region goes to zero.

2 Description of the problem

An infinite plate with a symmetrically located spherical cavity of radius R is shown in Fig.2 with the origin of the adopted cylindrical frame of reference located at the centre of the cavity. The geometry of the problem can also be considered as representative of a small cavity placed between two large ones with infinite radiuses. The plate is subjected to uniform radial tension at infinity. The presence of the cavity creates two narrow regions, symmetrically located with respect to the $r - \theta$ plane. With the minimum thickness of each narrow region denoted by h_0, the thickness of the plate is $2a = 2(R + h_0)$. The problem is obviously axisymmetric as well as statically indeterminate.

A formal solution of this problem under much more general loading conditions has been obtained [11] considering an infinite flat layer uniformly
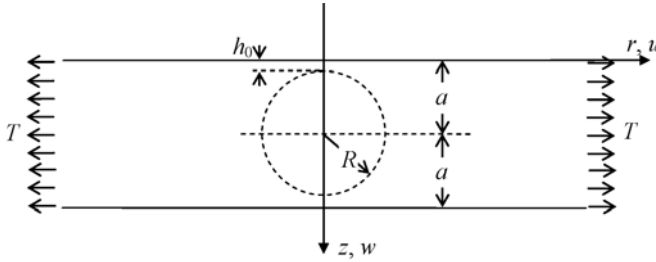
Figure 2: Centrally located spherical cavity in an infinite plate under uniform radial tension

compressed on both faces and also subjected to arbitrary coupled kinematic and traction conditions on the surface of the cavity. This general solution is very complex and does not seem to have been numerically implemented. More tractable solutions have been obtained in the case of uniform radial tension at infinity. Ling [12] derived the appropriate stress function satisfying the biharmonic equation for axisymmetric elasticity [13] in the form of an infinite series. Fox [14] represented the displacement vector also in the form of an infinite series and adopted an iterative procedure whereby each term was constructed from its predecessor. Neither of these solutions can be mathematically manipulated to relate explicitly the stress factors S and K to the minimum thickness h_0. Ling's solution was numerically implemented here in order to examine the trends for both σ_0 and σ_{max} as h_0 approaches zero. Such calculations contributed to the validation of an approximate expression for the limit value of the stress concentration factor K, whose derivation was the main objective of this paper. They also confirmed finite element results for σ_0 thus providing confidence in the proposed approximation for the amplification factor S.

The adopted methodology for obtaining K is similar to Koiter's approximate approach [2] with the simple beam or cylindrical shell theory here replaced by the Kirchhoff plate theory. The weakened part of the infinite plate $(0 \leq r \leq R)$ can be considered as two, symmetrically positioned circular plates of radius R and variable thickness

$$h = h_0 + R - \sqrt{R^2 - r^2}. \tag{5}$$

For $r << R$, Eq.(5) is simplified to

$$h \cong h_0 + \frac{r^2}{2R}. \qquad (6)$$

The stress and deformation fields near the centre of each narrow region are determined by solving the partial differential equations governing in-plane resultant forces N_r, N_θ and bending moments M_r, M_θ within that region.

3   Governing equations

The applied theory is based on Kirchhoff's thin plate hypothesis. A schematic view of a section by a plane through the axis of symmetry is shown in Fig.3. Referring to the notation of that figure, the axisymmetric displacement com-
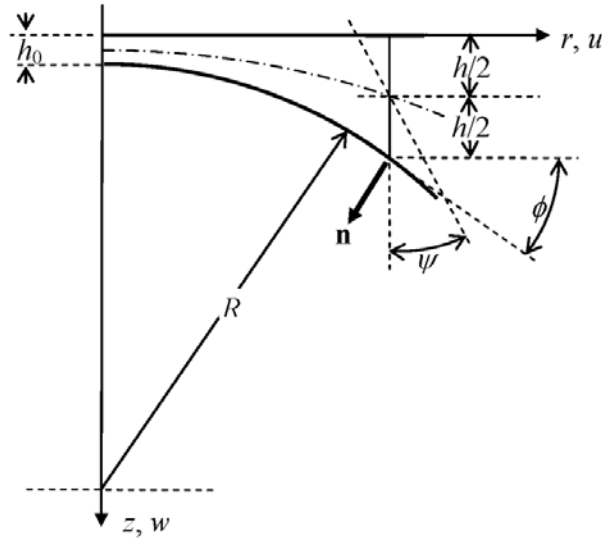

Figure 3: Enlarged view of a section of the narrow region by a plane through its axis of symmetry.

ponents $\hat{u}(r, z)$ and $\hat{w}(r, z)$ can be assumed as given by

$$\hat{u}(r, z) = u(r) + \psi(r) \left[z - \frac{h(r)}{2} \right], \quad \hat{w}(r, z) = w(r), \qquad (7)$$

where u is the radial displacement over the mid-surface of the plate and ψ the rotation of the cross section normal to the radial direction satisfying

$$\psi = -\frac{dw}{dr},$$

so that the shear strain relative to the adopted frame of reference vanishes. Thus, the non-vanishing normal strain components are given by

$$\varepsilon_r = \frac{du}{dr} + \left(z - \frac{h}{2}\right)\frac{d\psi}{dr} - \frac{1}{2}\frac{dh}{dr}\psi, \quad \varepsilon_\theta = \frac{u}{r} + \left(z - \frac{h}{2}\right)\frac{\psi}{r}. \tag{8}$$

Using the stress-strain relations of plane stress elasticity and the definition of the membrane forces leads to the constitutive relations

$$\begin{aligned}
N_r &= \frac{Eh}{1 - \nu^2}\left(\frac{du}{dr} + \nu\frac{u}{r} - \frac{1}{2}\frac{dh}{dr}\psi\right), \\
N_\theta &= \frac{Eh}{1 - \nu^2}\left(\frac{u}{r} + \nu\frac{du}{dr} - \frac{\nu}{2}\frac{dh}{dr}\psi\right),
\end{aligned} \tag{9}$$

where E is the Young's modulus. Similarly, expressions of the bending moments are obtained in terms of the deflection gradient as

$$\begin{aligned}
M_r &= \frac{Eh^3}{12(1 - \nu^2)}\left(\frac{d\psi}{dr} + \nu\frac{\psi}{r}\right), \\
M_\theta &= \frac{Eh^3}{12(1 - \nu^2)}\left(\frac{\psi}{r} + \nu\frac{d\psi}{dr}\right).
\end{aligned} \tag{10}$$

The equilibrium equations

$$\frac{dN_r}{dr} + \frac{N_r - N_\theta}{r} = 0, \tag{11}$$

$$\frac{dM_r}{dr} + \frac{M_r - M_\theta}{r} + \frac{N_r}{2}\frac{dh}{dr} = 0, \tag{12}$$

can be derived by considering the equilibrium of an infinitesimal plate element with sides normal to co-ordinate directions or by integrating the stress equations of axisymmetric elasticity through the plate thickness.

Eqs.(11) and (12) are transformed into ones for the mid-surface radial displacement u and deflection gradient ψ using constitutive relations (9)

and (10) and accounting for the approximation represented by Eq.(6). This process leads to the coupled differential equations

$$
\begin{aligned}
&\left(h_0 + \frac{r^2}{2R}\right)\frac{d^2u}{dr^2} + \left(h_0 + \frac{3r^2}{2R}\right)\frac{1}{r}\frac{du}{dr} - \left[h_0 + (1-2\nu)\frac{r^2}{2R}\right]\frac{u}{r^2} \\
&\qquad = \frac{1}{2R}\left(h_0 + \frac{r^2}{2R}\right)\left[r\frac{d\psi}{dr} + (2-\nu)\psi\right] + \frac{r^2}{2R^2}\psi,
\end{aligned}
\tag{13}
$$

$$
\begin{aligned}
&-\left(h_0 + \frac{r^2}{2R}\right)^2\left(\frac{d^2\psi}{dr^2} + \frac{1}{r}\frac{d\psi}{dr} - \frac{\psi}{r^2}\right) - \frac{3r}{R}\left(h_0 + \frac{r^2}{2R}\right)\left(\frac{d\psi}{dr} + \nu\frac{\psi}{r}\right) \\
&\qquad + \frac{3r^2}{R^2}\psi = \frac{6r}{R}\left(\frac{du}{dr} + \nu\frac{u}{r}\right).
\end{aligned}
\tag{14}
$$

Defining length parameter $b = \sqrt{2h_0 R}$ and introducing the dimensionless variable

$$
\rho = \frac{r}{b},
$$

Eqs.(13) and (14) are transformed to

$$
\begin{aligned}
&\rho^2(1+\rho^2)u'' + \rho(1+3\rho^2)u' - [1+(1-2\nu)\rho^2]u \\
&\qquad = h_0(1+\rho^2)[\rho\psi' + (2-\nu)\psi] + 2\rho^2\psi,
\end{aligned}
\tag{15}
$$

$$
\begin{aligned}
&-(1+\rho^2)^2\left(\psi'' + \frac{1}{\rho}\psi' - \frac{\psi}{\rho^2}\right) - 6\rho(1+\rho^2)\left(\psi' + \nu\frac{\psi}{\rho}\right) \\
&\qquad + 12\rho^2\psi = \frac{12}{h_0}(\rho u' + \nu u),
\end{aligned}
\tag{16}
$$

where dashes represent derivatives with respect to ρ.

Solution trends are sought from the coupled system of differential equations (15) and (16) as h_0 becomes arbitrarily small. The form of these equations suggests an iterative solution process whereby Eq.(15) is initially solved with its right-hand side neglected. The mid-surface radial displacement thus obtained can then be substituted to Eq.(16) to yield an initial solution for the deflection gradient. The latter can be introduced back to the right-hand side of Eq.(15) and a second iteration attempted to improve solution accuracy.

4   Mid-surface membrane problem

As explained in the previous section, only the complementary function for Eq.(15) is initially sought; the particular integral depends on h_0 and therefore its significance diminishes as $h_0 \to 0$. Since $u(0) = 0$, only a regular series solution is sought in the form [15]

$$u = \sum_{k=0}^{\infty} c_k \rho^{\ell+k}. \tag{17}$$

Substituting Eq.(17) into the left-hand side of Eq.(15) leads to the characteristic equation

$$\sum_{k=0}^{\infty} [(\ell+k)^2 - 1]c_k \rho^{\ell+k} + \sum_{k=2}^{\infty} [(\ell+k-2)(\ell+k) - (1-2\nu)]c_{k-2}\rho^{\ell+k} = 0. \tag{18}$$

Setting the coefficients of equal powers of ρ equal to zero yields the condition

$$[(\ell+k)^2 - 1]c_k + [(\ell+k-2)(\ell+k) - (1-2\nu)]c_{k-2} = 0, \tag{19}$$

which is valid for $k \geq 2$. For $k = 0$ and $k = 1$, Eq.(18) is satisfied if

$$(\ell^2 - 1)c_0 = 0, \tag{20}$$

$$[(\ell+1)^2 - 1]c_1 = 0, \tag{21}$$

which are simultaneously satisfied for either $\ell = \pm 1$ and $c_1 = 0$ or $\ell = 0$, $\ell = -2$ and $c_0 = 0$. Adopting the first combination of values, it is immediately obvious that k must be even. It is also noted that, for $k = 2$, Eq.(19) becomes

$$[(\ell+2)^2 - 1]c_2 + [\ell(\ell+2) - (1-2\nu)]c_0 = 0,$$

which can be solved for c_2 only if $\ell = 1$. Thus, the radial displacement can be expressed as

$$u = \rho \sum_{m=0}^{\infty} c_{2m}\rho^{2m} \tag{22}$$

with the coefficients c_{2m} obtained from the recurrence relation

$$c_{2m} = -\frac{2m^2 - 1 + \nu}{2m(m+1)}c_{2m-2}, \tag{23}$$

which follows from Eq.(19).

If the combination $c_0 = 0$, $\ell = 0$ and $\ell = -2$ is adopted, then k is shown to be odd and condition (19) for $k = 3$:

$$[(\ell + 3)^2 - 1]c_3 + [(\ell + 1)(\ell + 3) - (1 - 2\nu)]c_1 = 0$$

can be solved for c_3 only if $\ell = 0$. Thus, the resulting solution for u is identical to that given by Eq.(22).

It is worth noting that c_{2m} are independent of h_0; thus, the series represented by Eq.(22) can be expressed as a function of ρ and ν:

$$u = c_0 f(\rho, \nu). \tag{24}$$

It is obvious from Eq.(23) that c_{2m} form a slowly decaying sequence, therefore the series solution (22) converges for $\rho < 1$. Since

$$\frac{r}{R} < \sqrt{\frac{2h_0}{R}}$$

within that range, the approximation represented by Eq.(6) is valid provided $h_0 << R$.

Substituting the solution for the displacement given by Eq.(22) into the first of Eqs.(9) gives

$$N_r = \frac{Eh_0}{b(1 - \nu^2)}(1 + \rho^2) \sum_{m=0}^{\infty} c_{2m}(2m + 1 + \nu)\rho^{2m}. \tag{25}$$

Thus the membrane force at the centre is given by

$$N_0 = N_r(0) = \frac{Eh_0 c_0}{b(1 - \nu)}. \tag{26}$$

Re-arranging,

$$c_0 = \frac{b(1 - \nu)}{E}\frac{N_0}{h_0} = \frac{b(1 - \nu)}{E}\sigma_0. \tag{27}$$

4.1   Mid-surface bending problem

Substitution of the solution for u, given by Eq.(22), transforms the right-hand side of Eq.(16) to

$$\frac{12}{h_0}(\rho u' + \nu u) = \frac{12}{h_0} \sum_{m=0}^{\infty} c_{2m}(2m + 1 + \nu)\rho^{2m+1},$$

which suggests a series solution for Eq.(16) of the form

$$\psi = \sum_{m=0}^{\infty} \beta_{2m}\rho^{2m+1}(1+\rho^2)^{-2m-1}. \tag{28}$$

The solution given by Eq.(28) is similar to that adopted for Koiter's stress concentration problems [2]; it satisfies the symmetry condition $\psi(0) = 0$ and tends to zero for large ρ. The latter condition is consistent with the expectation of a clamped edge away from the z axis. Coefficients β_{2m} can be determined from the characteristic equation obtained by substituting the assumed solution for ψ , given by Eq.(28), namely,

$$
\begin{aligned}
&- 2\sum_{m=1}^{\infty} \beta_{2m}m(m+1)\rho^{2m-2}(1+\rho^2)^{-2m+1} \\
&+ \sum_{m=0}^{\infty} \beta_{2m}[(4m+1)(2m+1) - 3\nu]\rho^{2m}(1+\rho^2)^{-2m} \\
&- 4\sum_{m=0}^{\infty} \beta_{2m}(2m-1)(m+2)\rho^{2m+2}(1+\rho^2)^{-2m-1} \\
&= \frac{6}{h_0}\sum_{m=0}^{\infty} c_{2m}(2m+1+\nu)\rho^{2m}.
\end{aligned}
\tag{29}
$$

Introducing the expansion

$$(1+\rho^2)^{-k} = 1 - k\rho^2 + \frac{k(k+1)}{2}\rho^4 - \frac{k(k+1)(k+2)}{6}\rho^6 + \dots$$

into Eq.(29) and setting the coefficients of same powers of ρ equal to zero generates a system of infinite equations for β_{2m}. Retaining only the first two terms of the series in Eq.(28), the infinite system of equations derivable from Eq.(29) reduces to

$$(1 - 3\nu)\beta_0 - 4\beta_2 = A, \tag{30}$$

$$8\beta_0 + (19 - 3\nu)\beta_2 = -\frac{3+\nu}{4}A, \tag{31}$$

where

$$A = \frac{6(1+\nu)}{h_0}c_0.$$

The above system of equations provides the following solution for β_0:

$$\beta_0 = \frac{4(4 - \nu)}{3(1 - \nu)(17 - 3\nu)} A,$$

Substituting Eq.(28) into the first of expressions (10) gives

$$M_r = \frac{Eh_0^3}{12(1 - \nu^2)b} \sum_{m=0}^{\infty} \beta_{2m} \Big[(2m + 1 + \nu)(1 + \rho^2) - 2(2m + 1)\rho^2 \Big] \rho^{2m}(1 + \rho^2)^{-2m+2}.$$

Hence, at the centre of the plate,

$$M_r(0) = M_0 = \frac{Eh_0^3}{12(1 - \nu^2)b}(1 + \nu)\beta_0. \tag{32}$$

Substituting the expression for β_0 into Eq.(32) gives

$$M_0 = \frac{2(1 + \nu)(4 - \nu)}{3(1 - \nu)(17 - 3\nu)} h_0 N_0.$$

The extreme values of the radial stress at the centre of the narrow region are therefore given by

$$\sigma_r|_{\pm\delta/2} = \frac{N_0}{h_0} \pm \frac{6M_0}{h_0^2} = \left[1 \pm \frac{4(1 + \nu)(4 - \nu)}{(1 - \nu)(17 - 3\nu)} \right] \sigma_0. \tag{33}$$

According to the notation of Fig.3, maximum σ_r occurs at the bottom face of the narrow region, hence the stress concentration factor there is given by

$$K = \frac{(11 + \nu)(3 - \nu)}{(1 - \nu)(17 - 3\nu)}. \tag{34}$$

The approximation for K, provided by Eq.(34), can be further improved by retaining additional terms of the series in Eq.(28) and generating from Eq.(29) a consistent system of equations governing the respective coefficients β_{2m}.

5 Mean stress at minimum thickness

5.1 Exact solution

As already pointed out, Ling [12] derived the stress function of this axisymmetric problem in the form of infinite series; all stress components can be obtained by introducing this stress function into the respective differential operators [13]. The expression for $\sigma_r(r = 0, z) = \sigma_\theta$ $(r = 0, z)$ is of particular interest here since it provides $\sigma_{max} = \sigma_r$ $(r = 0, z = R)$ as well as the mean stress

$$\sigma_0 = \frac{N_0}{h_0} = \frac{1}{h_0} \int\limits_R^a \sigma_r(0, z)dz, \tag{35}$$

which allow the evaluation of both the amplification and concentration factors. The evaluation of σ_z $(r = 0, z)$ is also a useful validation result. This stress satisfies $\sigma_z(0, R) = \sigma_z$ $(0, a) = 0$; therefore, it becomes very small as $h_0 = a - R$ approaches zero. As such, it provides an additional criterion for assessing the reliability of the truncated solution.

The coefficients of the series solution satisfy a system of infinite linear algebraic equations and are implicit functions of

$$\lambda = \frac{R}{a} = \frac{1}{1+\delta}.$$

These coefficients were evaluated through the solution of truncated systems implemented via a FORTRAN program using double precision accuracy. For a given λ, the accuracy of the solution depended on the order of truncation of the infinite series. The number of terms required to achieve a specified degree of accuracy increased sharply as λ approached 1 or δ approached 0. Eventually, for very small values of δ, convergence could not be achieved whatever the order of truncation.

5.2 Solution for zero minimum thickness

The apparent divergence of the exact solution as $h_0 \to 0$ is an indication of a possible singular stress field at $r = 0$. Such singularity is easily detected in statically determinate stress concentration problems such as that described in Fig.1 for which stress amplification is governed by Eq.(2). In the case of a circular hole near a free surface, σ_0 was shown to grow with $(R/h_0)^{1/2}$ as $h_0 \to 0$ [8, 16]. Since, in the present problem, the exact solution fails

to provide the limit value of σ_0 as $h_0 \to 0$, this limit is sought by resorting to the equations of the approximate analysis presented in Section 3. Thus, σ_0 is determined from Eq.(13) with h_0 set equal to zero, that is, from the solution of the differential equation

$$r^2 \frac{d^2 u}{dr^2} + 3r \frac{du}{dr} - (1 - 2\nu)u = \frac{r^2}{2R} \left[r \frac{d\psi}{dr} + (4 - \nu)\psi. \right] \tag{36}$$

Since $\psi(0) = 0$, it is reasonable to assume a power series expansion for ψ in the form

$$\psi = \sum_{k=1}^{\infty} \psi_k r^k.$$

Then, the general solution of Eq.(36) is easily obtained as

$$u = Ar^\alpha + \sum_{k=1}^{\infty} b_k r^{k+2}, \tag{37}$$

where $0 < \alpha = \sqrt{2(1 - \nu)} - 1 < 1$ for $0 \le \nu < 0.5$ and

$$b_k = \frac{k + 4 - \nu}{2R(k^2 + 6k + 7 + 2\nu)} \psi_k.$$

Substituting Eq.(37) into the first of constitutive relations (9) gives

$$\sigma_r = \frac{N_r}{h} = \frac{E}{1 - \nu^2} \left[A(\alpha + \nu)r^{\alpha-1} + \sum_{k=1}^{\infty} \frac{1 - \nu^2}{2R(k^2 + 6k + 7 + 2\nu)} \psi_k r^{k+1} \right].$$

This solution confirms that σ_r is singular at $r = 0$, therefore $\sigma_0 = \sigma_r(0)$ must also go to infinity as h_0 approaches zero. The rate of growth of σ_0 with diminishing h_0 is not however revealed. Such information is not provided by the approximate solution represented by Eq.(22) since its range of validity vanishes as h_0 becomes zero.

5.3   Finite element modelling

Finite element (FE) modelling was attempted as a possible means of obtaining σ_0 and σ_{max} for values of λ even closer to 1 than those causing divergence of the exact series solution. FE results would also provide further insight

into the stress and displacement distributions of the problem and contribute to the validation of the obtained approximate analytical results.

The numerical work was based on ANSYS, a general purpose FEM package [17]. The analyses were performed for $\delta = 10^{-n}$, with n taking four integer values from 1 to 4. The finite element models were built using plane 8-node quadrilateral elements with the axisymmetric analysis option; a typical meshed model is shown in Fig.4 for the case $\delta = 10^{-2}$. The mesh was
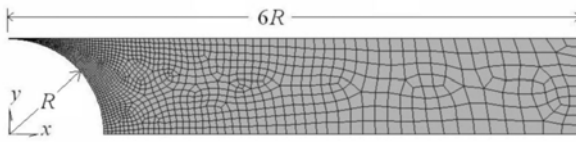
Figure 4: Finite element model: $x - y$ plane stress for the strip, x-axisymmetric for the bar and y-axisymmetric for the plate problem.

refined until a stable solution was obtained. In all cases analysed, there were 20 elements across the section of minimum thickness and a consistent mesh density within the narrow zone. Systematic mesh control ensured a gradual element size transition from the minimum at $r=0$ to the maximum at the model periphery. The horizontal dimension of the model was chosen such that the results would be insensitive to any further enlargement of the model in that direction. As with the numerical implementation of the exact series solution, the predicted variation of $\sigma_z(0, z)$ provided further evidence on the quality of the mesh.

6 Results and discussion

6.1 Validation

The particular ANSYS element type used can be easily adapted to plane stress conditions, which are applicable to the problem of a flat strip with symmetrically located hole [2, 4]. The same plate element can be used for axisymmetric analyses; thus the model shown in Fig.4 was also applied to the axisymmetric cylindrical bar problem [2] shown in Fig.1 by specifying the x-axis of the frame of reference shown in Fig.4 as the axis of symmetry. Thus the adopted FE modelling was initially validated through its application to

these two problems. In the case of the strip problem, the theoretical values for both S and K were almost exactly reproduced by FE for the initially adopted δ value of 10^{-1}. The corresponding results for the cylindrical bar reached almost exactly the predictions from Eqs.(2) and (4) for $\delta = 10^{-2}$.

FE results were then obtained for the problem under consideration here, that is, the axisymmetric problem shown in Fig.2 for which the y-axis in Fig.4 becomes the z-axis of symmetry. These results were validated by their comparison with those obtained from the exact series solution [12]. It was thus necessary to duplicate first and then extend Ling's results so that there is greater overlap between them and the respective FE predictions; such results also helped in establishing trends for the stress amplification and concentration as λ approaches 1. The variation of $\sigma_{max}/T = KS$ with λ for $\nu = 0.25$ is shown in Fig.5. It is worth noting that σ_{max}/T was given
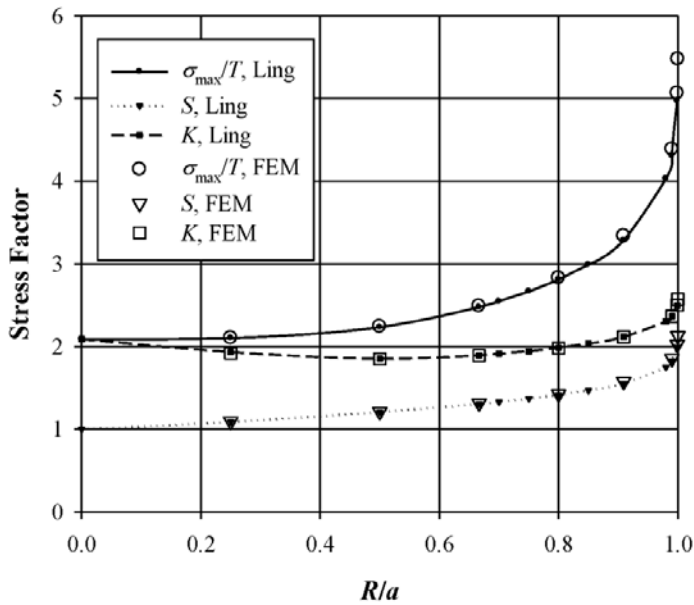

Figure 5: Variation of maximum stress, concentration and amplification factors with cavity radius

for only $\lambda = 0.25$ and $\lambda = 0.5$ in the original paper by Ling. The case of $\lambda = 0$ corresponds to that of a cavity in an infinite medium for which the

exact theoretical result $\sigma_{max}/T = 12/(7-5\nu)$ applies. Ling's series solution is here extended over almost the complete range of λ, that is, for up to $\lambda \cong 0.999$ corresponding to $\delta = 10^{-3}$; beyond this value, the existing FORTRAN program could not produce convergent results. This could, perhaps, have been achieved through additional programming and computational effort but it was not pursued since it was not expected to yield information of commensurate importance.

The stress ratio σ_{max}/T was split into its two factors K and S using Eq.(35) to compute the mean stress σ_0. The plots of these new results, extracted from the series solution, are also shown on the graph of Fig.5. The variation of K deserves particular attention since it contrasts the experience from other well known stress concentration problems such as that of a hole in a finite or semi-infinite plate or a spherical cavity in a cylindrical bar. In those problems, K is largest for the infinite solid and drops to its minimum value as the boundary of the hole or cavity approaches the solid boundary. In the present problem, K initially drops for values of λ up to, approximately, 0.5 but then rises again towards a value greater than that for the infinite solid. This may be due to the extremely slow growth rate of stress amplification S with decreasing δ; while, in the case of the aforementioned problems, S goes to infinity as δ^{-1} or $\delta^{-1/2}$.

The respective FE results for both S and K as well as σ_{max}/T, also shown in Fig.5, are in excellent agreement with and follow the trends of those obtained from the analytical, series solution. As a further comparison between the analytical and FE predictions, the variation of σ_z at $r = 0$, that is, through minimum narrow zone thickness, is presented in Fig.6 for $\lambda \cong 0.999$ or $\delta = 10^{-3}$. Considering that the maximum σ_z is three orders of magnitude smaller than the corresponding σ_{max}, the agreement can be considered satisfactory. The analytical solution was obtained by retaining 500 terms in the series but a small error at $(0,R)$, where σ_z should vanish, still persists while this is absent from the respective FE prediction, which was obtained using 7,040 elements. In the case of $\delta = 10^{-4}$, it proved impossible to reach a convergent series solution while FE modelling with a rational mesh size distribution provided answers consistent with the established trends shown in Fig.5 as well as a smooth variation for $\sigma_z(0,z)$, similar to that shown in Fig.6, but by one order of magnitude smaller.

Since the derivation of Eq.(34) for the concentration factor K depends, according to Eq.(16), on the prior knowledge of the radial displacement
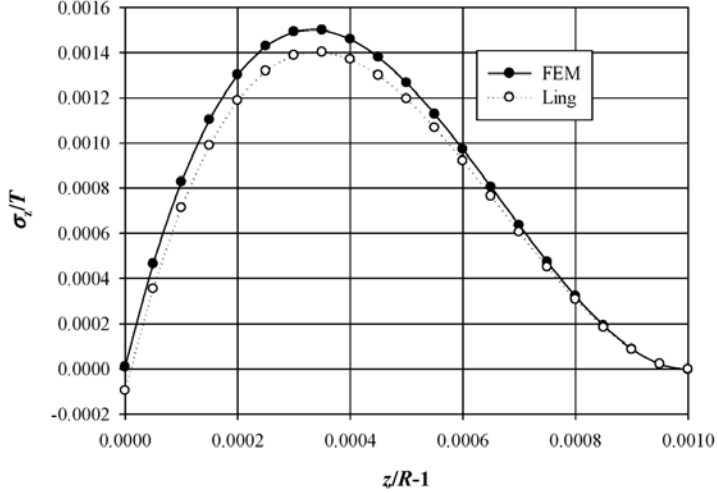
Figure 6: Variation of σ_z through minimum thickness for $h_0/R = 0.001$, $\nu = 0.25$

$u(r)$, the accuracy of the approximate solution, Eq.(22), was also examined by comparing its predictions with respective FE output. The variation of the ratio u/c_0 obtained from Eq.(22) and three FE analyses is plotted against the dimensionless co-ordinate ρ in Fig.7. This figure shows the consistency of the FE results as well as their excellent agreement with the predictions of the present approximate analysis for low values of ρ, that is, for $\rho < 0.2$. The increasing discrepancy between the two solutions for $\rho > 0.2$ can be attributed to the influence of the right-hand side of Eq.(15), which was not accounted for in the solution of that equation and should have affected the higher-order terms of expansion (22).

6.2   Stress concentration factor

The estimates of stress concentration factor K using the approximate expression in Eq.(34) are plotted in Fig.8 against Poisson's ratio ν together with the predictions of the FE analyses for various δ. Results from the exact series solution are not shown since they are almost identical to the FE predictions for any value of ν. It should also be noted that only the FE analysis
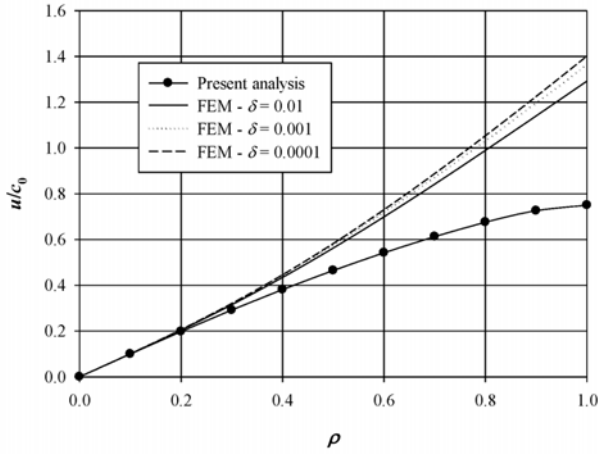
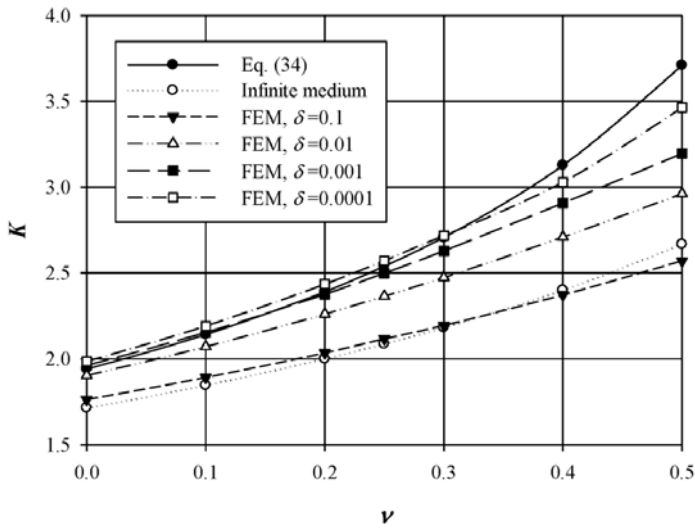Figure 7: Approximate analytical and FEM results for mid-surface radial displacement ($\nu = 0.3$)

Figure 8: Analytical and FEM results for the stress concentration factor

produced results in the case of $\delta = 10^{-4}$. The FE predictions show a very clear trend towards the approximate analytical result as δ approaches zero. Considering the degree of approximation in the derivation of Eq.(34), its consistency with FE results can be characterised as satisfactory. With the confidence in FE results gained from their agreement with those obtained from Ling's solution, it may be concluded that formula (34) slightly under-estimates K for $\nu < 0.3$ and overestimates it for $\nu > 0.3$. As pointed out in Section 4.1, the approximation can be improved by generating and solving a larger system of equations for β_{2m} but this would be at the expense of the simple, closed form solution (34). The stress concentration factor for a cavity in an infinite solid is also plotted in Fig.8 noting again that it is lower than that given by Eq.(34) in contrast to previous experience with other well known stress concentration problems.

6.3   Stress amplification factor

Trends for the amplification factor S are detected by examining how the results for N_0 relate to changing h_0. For this purpose, $N_0/(aT)$ is plotted against h_0/a on a log-log scale for three values of ν, as shown in Fig.9. The
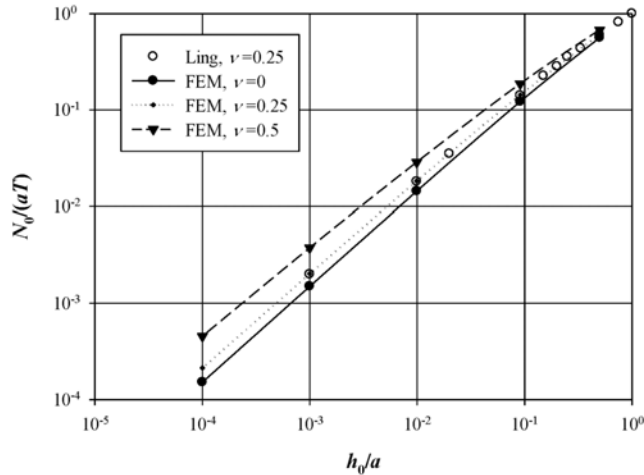

Figure 9: Variation of the central radial force with minimum narrow zone thickness

exact solution is included only for $\nu = 0.25$ just to demonstrate again its excellent agreement with the FE results. Only the latter are used systematically since they include an additional point along each of the curves in Fig.9. The gradients of these curves appear to approach a value slightly less than unity as h_0/a goes to zero. If the limits of these gradients were equal to unity, then the relation between N_0 and h_0 would have become linear and σ_0 would have a constant limiting value. This however contradicts the earlier theoretical prediction that this stress should become infinite at $h_0 = 0$. It is therefore reasonable to assume that, as h_0/a goes to zero, the dominant term in the expression for N_0 in terms of h_0 would have the form

$$\frac{N_0}{aT} \cong C \left(\frac{h_0}{a} \right)^{1-\gamma}. \tag{38}$$

where γ is a small positive number depending on the Poisson's ratio ν. From Eq.(38), the stress amplification factor is obtained as

$$S = \frac{\sigma_0}{T} \cong C \left(\frac{h_0}{a} \right)^{-\gamma}. \tag{39}$$

It is understood that only approximate bounds for parameters C and γ can be obtained from Fig.9. Such lower bounds for C and upper bounds for γ for various values of ν are listed in Table 1. The curvature trends in Fig.9 clearly indicate that S is overestimated when the C and γ values from Table 1 are substituted in Eq.(39).

Table 1: Approximate values for the parameters appearing in Eqs.(38) and (39)

ν	C	γ
0	1.444	0.0051
0.1	1.551	0.0090
0.2	1.677	0.0161
0.3	1.815	0.0289
0.4	1.943	0.0516
0.5	2.158	0.0806

A numerical example is used to demonstrate the degree of singularity arising from Eq.(39). For $h_0 = 1$ Å, which is of the order of an atomic diameter, and $a = 1$ m, Eq.(39) applied with C and γ values from Table 1 predicts S values ranging from 1.62 for $\nu = 0$ to 13.80 for $\nu = 0.5$. For all practical purposes therefore, S can be considered as having a finite limit in an elastic continuum; this limit would depend on the ratio of a characteristic microstructural dimension to the cavity radius or the plate thickness.

A similar problem that may provide clues about plausible, practical limit values for S is the case of a centrally located cylindrical cavity in a plate of thickness $2a$, as shown in Fig.10. The cavity is capped by two circular
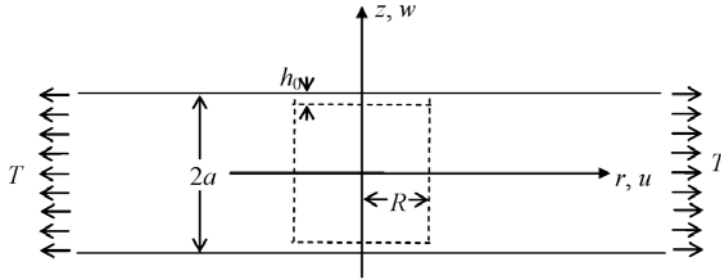

Figure 10: Centrally located cylindrical cavity in an infinite plate under uniform radial tension

membranes of uniform thickness h_0 and its axis is aligned with the z axis of the cylindrical frame of reference so that its length is $2(a - h_0)$. Keller's approach [10] is easily applicable to this simpler problem. If h_0 is considered infinitesimally small, the end caps would have negligible stiffness and the radial displacement at their periphery should be the same as that of the lateral surface of the cavity where the hoop stress is equal to $2T$, while the caps themselves are under uniform stress $\sigma_r = \sigma_\theta = \sigma_0$, apart from the stress concentration in a small volume around their periphery.

Compatibility of displacement at the cap periphery gives

$$S_{cc} = \frac{\sigma_0}{T} = \frac{2}{1 - \nu}. \tag{40}$$

It is worth noting that the amplification factor S_{cc} for the cylindrical cavity, given by Eq.(40), is an exact upper limit as h_0 approaches zero. The values

of S_{cc} obtained from Eq.(40) are plotted in Fig.11 together with the respective FE estimates for the spherical cavity problem. Stress amplification in
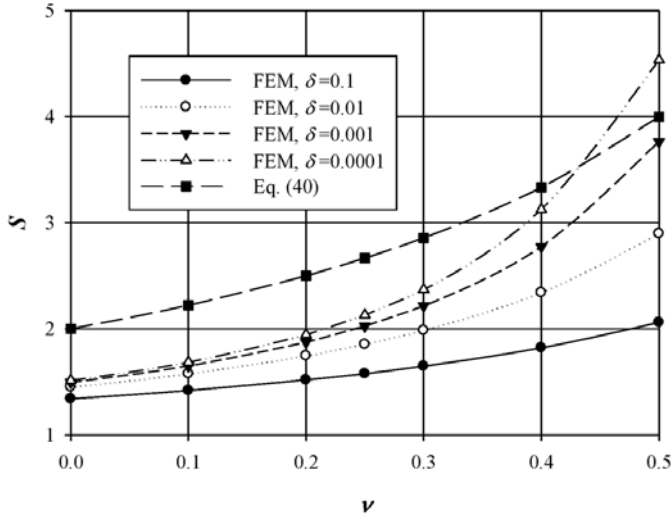

Figure 11: Analytical and FEM results for the stress amplification factor

the latter case is intuitively expected to be less than predicted by Eq.(40) due to the greater rigidity of the circular plates with non-uniform thickness. This is confirmed by the FEM results of Fig.11 for $\nu < 0.4$. However, as the material becomes less compressive, stress amplification in the spherical cavity problem becomes more pronounced and the respective S factor eventually exceeds S_{cc} for relatively high h_0/a ratios.

7 Concluding remarks

The attempted derivation of an approximate solution for a three dimensional stress concentration problem illustrated the differences between this and similar two dimensional problems. A basic difficulty arises from the static indeterminacy of the problem. The approximate model for the narrow region, a circular plate of variable thickness in the present case, is certainly more complex than the beam approximation employed earlier in

two-dimensional problems.

These difficulties were partially overcome and it was possible to obtain a reasonable approximation for the conventional stress concentration factor. Trends for the stress amplification resulting from diminishing thickness of the narrow region were identified through the numerical implementation of an exact, series solution and a finite element analysis. These solutions also provided stress and displacement results consistent with those predicted by the proposed approximate method. The interesting outcomes of the exact solution implementation and FE modelling are that (i) the limit value of the stress concentration factor as the minimum thickness of the narrow region goes to zero is higher than that for a cavity in an infinite medium in contrast to experience with other two or three-dimensional stress concentration problems and (ii) the singularity of stress amplification with diminishing minimum thickness is very mild to the extent that the amplified stress can be considered finite within the context of a continuum theory.

There is a multitude of three-dimensional configurations of cavities in solids under uni-axial and multi-axial tension. As in two-dimensional problems, the analysis of various configurations may lead to a wide range of stress concentration and amplification factors, even to solutions with more pronounced singularities as the minimum thickness of the narrow zones considered approaches zero. The trends identified from the results presented in this paper should not therefore be generalised but there is scope for the modelling methodology to be adapted to other geometrical arrangements leading to a broader spectrum of answers.

The presented methodology can be easily extended to axisymmetric cavity problems for which exact solutions are available such as that for a plate under circular bending [18] and a semi-infinite space [19] or an infinite space with two cavities [19, 20] under remote radial tension. Solutions also exist for plate problems with non-axisymmetric loading such as uniaxial tension [21, 22, 23] and plane bending [24, 25] for which modified approximate solutions need to be developed. Finally, another interesting recent development in the analysis of stress concentration problems is the consideration of surface stress effects [26, 27], which would be quite relevant in the study of stresses in three dimensional narrow regions with the slow rate of stress amplification identified in the present paper.

Acknowledgement

References

[1] Timoshenko SP, Goodier JN. Theory of Elasticity, Third Edition. New York: McGraw-Hill; 1982.

[2] Koiter WT. An elementary solution of two stress concentration problems in the neighbourhood of a hole. Q Appl Math. 1957;15:303-8.

[3] Markenscoff X. Stress amplification in the neighborhood of an eccentric large hole in a strip in tension. Z Angew Math Phys. 2000;51:550-4.

[4] Lubarda VA, Markenscoff X. Stress magnification due to stretching and bending of thin ligaments between voids. Arch Appl Mech. 2006;76:295-310.

[5] Jeffery GB. Plane stress and plane strain in bipolar coordinates. Philos Trans R Soc A-Math Phys Eng Sci. 1920;221:265-93.

[6] Mindlin RD. Stress distribution around a hole near the edge of a plate under tension. Exp Stress Anal. 1948;5:56-67.

[7] Markenscoff X, Dundurs J. Amplification of stresses in thin ligaments. Int J Solids Struct. 1992;29:1883-8.

[8] Callias CJ, Markenscoff X. Singular asymptotics analysis for the singularity at a hole near a boundary. Q Appl Math. 1989;47:233-45.

[9] Sternberg E, Sadowsky MA. On the axisymmetric problem of the theory of elasticity for an infinite region containing two spherical cavities. J Appl Mech-Trans ASME. 1952;74:19-27.

[10] Keller JB. Stresses in narrow regions. J Appl Mech-Trans ASME. 1993;60:1054-6.

[11] Kaufman RN. Solutions of some boundary value problems of static theory of elasticity for a layer with a spherical cavity. Appl Math Mech. 1958;22:451-65.

[12] Ling C-B. Stresses in a stretched slab having a spherical cavity. J Appl Mech-Trans ASME. 1959;81:235-40.

[13] Love AEH. A Treatise on the Mathematical Theory of Elasticity, Fourth Edition. 4th ed. New York: Dover Pubications; 1944.

[14] Fox N. Torsion-free stress systems in a thick plate containing a spherical cavity. Q J Mech Appl Math. 1960;13:228-46.

[15] Ince EL. Ordinary Differential Equations. New York: Dover Publications; 1956.

[16] Duan ZP, Kienzler R, Herrmann G. An integral-equation method and its application to defect mechanics. J Mech Phys Solids. 1986;34:539-61.

[17] ANSYS. ANSYS Resease 11.0 ed. Canonsburg, PA 15317: ANSYS, Inc.; 2008. p. ANSYS Academic Research, Release 11.

[18] Ling C-B, Tsai C-P. Stresses in a slab having a spherical cavity under circular bending. J Appl Mech-Trans ASME. 1960;82:169-86.

[19] Tsuchida E, Nakahara I. Three-dimensional stress concentration around a spherical cavity in a semi-infinite elastic body. Bull Jpn Soc Mech Eng. 1970;13:499-508.

[20] Hamada M, Kodama J. Axisymmetric tension of an infinite body containing two spherical cavities. Bull Jpn Soc Mech Eng. 1985;28:408-13.

[21] Tsuchida E, Nakahara I. Stress concentration around a spherical cavity in a semi-infinite elastic body under uniaxial tension. Bull Jpn Soc Mech Eng. 1974;17:1207-17.

[22] Tsuchida E, Nakahara I. Three-dimensional stress concentration around a spherical cavity in a thick plate under uniaxial tension. Bull Jpn Soc Mech Eng. 1976;19:1107-14.

[23] Lee DS. Stress-analysis of a stretched slab having a spherical cavity under unidirectional tension. Int J Solids Struct. 1993;30:2709-27.

[24] Lee DS. Bending of an elastic slab having a spherical cavity. Eur J Mech A-Solids. 2004;23:865-75.

[25] Tsuchida E, Nakamura M, Nakahara I. Stresses in an elastic thick plate with a spherical cavity under transverse bending. Bull Jpn Soc Mech Eng. 1976;19:849-56.

[26] He LH, Li ZR. Impact of surface stress on stress concentration. Int J Solids Struct. 2006;43:6208-19.

[27] Hui SL, Shen SP. Analysis of the interaction between two nanovoids using bipolar coordinates. Comput Model Eng Sci. 2008;30:57-64.

Amplifikacija napona u trodimenzionalnim uskim zonama izazvanih šupljinama

U radu se tretira naponska amplifikacija izazvana prisustvom sferičnog materijalnog otvora u blizini konture elastično opterećenog čvrstog tijela. Predložena aproksimativna analiza daje raspored napona i pomeranja u uskoj zoni ligamenta usled ravnomernog istezanja. Analiza je bazirana na modelu kružne ploce neravnomerne debljine, koja poseduje membransku i savojnu krutost. Izvedeni izraz za faktor koncentracije napona u dobroj je saglasnosti sa rezultatima egzaktne analize i metode konačnih elemenata.